



# Quasielastic and inelastic neutron scattering study of the hydration of monoclinic and triclinic tricalcium silicate

Vanessa K. Peterson<sup>a,b,\*</sup>, Craig M. Brown<sup>a,b,\*</sup>, Richard A. Livingston<sup>c</sup>

<sup>a</sup> Center for Neutron Research, National Institute of Standards and Technology, 100 Bureau Drive MS 8562, University of Maryland, Gaithersburg, MD 20899-8562, USA

<sup>b</sup> Department of Materials Science and Engineering, University of Maryland, College Park, MD 20742-2115, USA

<sup>c</sup> Federal Highway Administration, HRDI-05, McLean, VA 22101, USA

Received 8 August 2005; accepted 16 February 2006

## Abstract

The hydration of Mg-stabilized triclinic and monoclinic tricalcium silicate samples were studied using quasielastic neutron scattering to follow the fixation of hydrogen into the reaction products and by applying hydration models to the data. The quantity of  $\text{Ca}(\text{OH})_2$  produced during hydration was also determined using inelastic neutron scattering. The monoclinic form was found to be intrinsically less reactive than the triclinic form. The monoclinic form was also confirmed to produce more product than the triclinic form after 50 h, a process found to occur through a longer, rather than earlier, nucleation and growth regime. Results indicated an increase in the permeability of the hydration layer product relative to the triclinic form and the increase in the length of the nucleation and growth regime was thus attributed to an alteration in morphology or structure of the hydration layer product, extending the time for diffusion limited mechanics to be reached.

© 2006 Elsevier B.V. All rights reserved.

**Keywords:** Quasielastic neutron scattering; Inelastic neutron scattering; Tricalcium silicate; Cement

## 1. Introduction

Cement paste is formed when cement clinker, a complex mixture, reacts with water and a small amount of gypsum, gaining strength for use in construction and other applications. The most abundant and mechanically important component of cement, tricalcium silicate ( $\text{C}_3\text{S}^1$ ), has polymorphs which are present in cement through ion-stabilization. Hydrated mortars prepared from various forms exhibit different strength properties; indirect methods have been used to demonstrate that these ion-stabilized forms have differing reaction rates and product morphologies [1–10]. This study uses quasielastic neutron scattering

(QENS) with the application of hydration models and inelastic neutron scattering to establish the variation in the mechanics of the hydration reactions of two common  $\text{C}_3\text{S}$  forms.

$\text{C}_3\text{S}$  reacts quickly with water and is responsible for early strength development. Pure  $\text{C}_3\text{S}$  exhibits polymorphism when heated and can be triclinic ( $T_1$ ,  $T_2$ , or  $T_3$ ), monoclinic ( $M_1$ ,  $M_2$ , or  $M_3$ ), or trigonal ( $R$ ). Whilst pure  $\text{C}_3\text{S}$  exists in the  $T_1$  form, higher temperature polymorphs of  $\text{C}_3\text{S}$  exist in cement, often simultaneously, through stabilization with ions such as commonly occurs with  $\text{Mg}^{2+}$  [11]. The exact structures and differences of these polymorphs and ion-stabilized forms is currently unknown. The effect of structural differences caused through this ion-stabilization on the hydration rate and resultant strength properties of the products are also unclear.

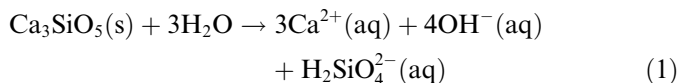
The hydration of  $\text{C}_3\text{S}$  can be described by three reaction regimes: initial hydrolysis, nucleation and growth,

\* Corresponding authors. Tel.: +61 434 501 710.

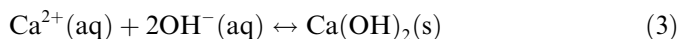
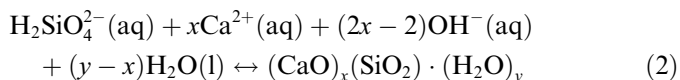
E-mail address: [v.peterson@chem.usyd.edu.au](mailto:v.peterson@chem.usyd.edu.au) (V.K. Peterson).

<sup>1</sup>  $\text{C}_3\text{S} = \text{Ca}_3\text{SiO}_5$  in cement chemists notation, where  $\text{C} = \text{CaO}$  and  $\text{S} = \text{SiO}_2$ .

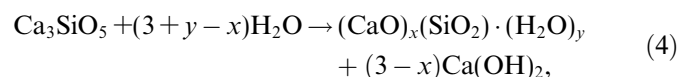
and diffusion limited hydration. Initial hydrolysis is the irreversible dissolution of the outer  $C_3S$  grain. During this process the  $C_3S$  grains rapidly release calcium and hydroxide ions, and a large amount of heat, according to the following irreversible, exothermic reaction:



The nucleation and growth period begins with the formation of calcium silicate hydrate (C–S–H) and calcium hydroxide:



Eqs. (2) and (3) usually proceed in the forward direction, resulting in the following idealized hydration reaction:



The Ca to Si ratio ( $x$ ) varies, although is usually close to 1.75 for a pure  $C_3S$  paste. The rate of C–S–H precipitation is equal to the rate of tricalcium silicate dissolution [12]. As the C–S–H layer thickens around the unreacted  $C_3S$  grains, it becomes increasingly difficult for water molecules to reach the  $C_3S$ . The rate of reaction is now controlled by the rate at which water molecules diffuse through the C–S–H layer, known as diffusion limited hydration. Hydration will continue as long as water and  $C_3S$  are present.

The compressive strength of the hydrated paste is related to the hydration mechanics that control the microstructure of the products that form. Many of the conclusions from earlier research linking  $C_3S$  form to reactivity with water are inconsistent [1–10], and pre-date recent discoveries linking particle size distribution(s) to the hydration mechanics and reaction rate [13,14]. Additionally, absolute identification of the crystal form has proven difficult to achieve since many forms have similar powder diffraction patterns.

A few studies exist that utilize techniques independent of these concerns, where particle size is irrelevant, and where crystal form was clearly identified by observation of crystal transition [5,7,8]. In the case of crystal modification through stabilization by Mg ions, thermodynamic calculations suggest that the Mg-stabilized monoclinic  $C_3S$  should be more reactive than pure  $C_3S$  since substitution of the  $Ca^{2+}$  by the smaller  $Mg^{2+}$  in the lattice gives a less stable and hence more reactive  $MgO_6$  group [5]. Stewart and Bailey also noticed that the influence of crystal form caused by the incorporation of foreign ions in  $C_3S$  is significant on its early hydration [5]. They observed the microstructural development of the hydration products and showed that a monoclinic  $C_3S$  form displayed a different hydration mechanism compared to the triclinic and trigonal forms studied, which were observed to have similar mechanisms.

The mechanism of rupture of the C–S–H layer on monoclinic grains was observed to occur by a process of lifting and peeling of sheets, unlike the random eruption of needle-like outgrowths observed in the triclinic and trigonal forms. Mascolo and Ramachandran concluded that dislocations, strains, or distortions in the lattice of  $C_3S$  stabilized with various ions seem to affect the nucleation and growth processes [7]. They also calculated the temperature of recrystallization to  $\beta$ -wollastonite of the C–S–H produced from various forms of  $C_3S$ , and concluded that the C–S–H produced varied with the  $C_3S$  form being hydrated. Thompson et al. investigated the reactivity of  $C_3S$  during annealing and determined an increase in the reactivity around the triclinic–monoclinic transition point, and discovered that the concentration of MgO used to prepare the  $C_3S$  also affect the hydration mechanism [8]. None of these works explain the observed differences between the mechanics of hydration of triclinic and monoclinic forms, which is the aim of this work, which clarifies the differences in terms of parameters describing the hydration kinetics.

During the hydration of the calcium silicates protons are transferred from the free water into the reaction products. Quasielastic neutron scattering (QENS) can be used to quantitatively determine the state of hydrogen in situ during the hydration of  $C_3S$ . Recently, QENS has been applied to the study of the hydration of Portland cement and its components, as a tool for the investigation of the hydration mechanics [13,15–23]. QENS spectra,  $S(Q, \omega)$ , are dependant on the magnitude of the scattering vector,  $Q$ , for the elastic contribution where  $Q = (4\pi/\lambda) \sin(\theta/2)$ , and  $\theta$  is the scattering angle, and energy transfer  $= \hbar\omega$ ,  $\hbar = h/2\pi$ , and  $h$  is Planck's constant. For a hydration reaction, the incoherent scattering is dominated by that from the hydrogen, present initially in the free water, and later in other states within the hydration products, including free, pseudo-bound, and completely bound states. The neutron scattering arising from H in each state differs in energy transfer characteristics.

Inelastic neutron scattering (INS) has also been used to investigate the in situ hydration of  $C_3S$  and determine the concentration of calcium hydroxide formed [19,23,24]. Inelastic neutron spectroscopy involves monitoring the energy change in a scattered neutron to gain information about vibrational modes within a sample. Comparison of the sample's spectrum to that of a chosen reference material allows characteristic frequencies to be associated to the sample. Calibration of the intensity of the sample peak(s) with a known mass of standard material allows the quantitative determination of the standard material in the sample. The main vibrational mode of calcium hydroxide, associated with the oscillation of the hydroxide group, at 41 meV, is chosen for its relatively high intensity, and for its ease of discrimination from modes arising from water and from the C–S–H that forms [19].

In this study, QENS and INS were applied to investigate the hydration of a triclinic and a monoclinic  $C_3S$ , as well as a 1 to 1 mixture of each form. The time-dependent free,

Table 1  
Composition as oxides in tricalcium silicate samples present in greater than 0.06 wt. %

Oxide	Triclinic (wt.%)	Monoclinic (wt.%)
SiO <sub>2</sub>	26.01	25.40
CaO	73.40	73.12
Al <sub>2</sub> O <sub>3</sub>	0.33	1.38
MgO	0.25	0.62

Table 2  
Summary of the particle size distribution in the tricalcium silicate samples

Size (μm)	Triclinic volume of particles below size (%)	Monoclinic volume of particles below size (%)
1	5.5	2.9
10	61	32
40	100	74
100	100	91
283	100	100

Volume listed to 2 significant figures.

constrained, and bound water QENS results were analyzed using a stretched exponential model for the nucleation and growth regime during early hydration times and a parabolic time dependence model for the diffusion limited growth period. The quantity of Ca(OH)<sub>2</sub> produced by each sample was determined using INS. Hydration of different C<sub>3</sub>S forms have not previously been investigated by these methods; new insights into the differences between hydration mechanics of these forms are presented.

## 2. Experimental section

### 2.1. Tricalcium silicate samples and hydration

Triclinic and monoclinic C<sub>3</sub>S powders stabilized using Mg were obtained from Construction Technology Laboratories (CTL, Skokie, IL<sup>2</sup>). Particle size analysis and X-ray fluorescence was conducted by CTL and chemical analyses reports were provided in terms of oxide composition (Tables 1 and 2). An average of four measurements was used to determine the average particle size and specific surface areas of the two samples. Each individual sample, and a 1 to 1 mixture of the two, was hydrated using distilled water and a water to cement component mass ratio of 0.4. Hydration took place inside a Teflon bag inside a rectangular aluminum hydration cell, at 30 °C.

### 2.2. QENS measurement

QENS measurements were carried out using the NIST Center for Neutron Research neutron time-of-flight Fermi Chopper Spectrometer (FCS) [25], with all samples at

30 °C. Each energy-transfer spectrum was derived from measurement of the time of flight distribution for scattered neutrons arriving at the instrument detectors after each incident neutron pulse. The sample thicknesses were approximately 1 mm in the hydration cell, which was placed at a 45° angle to the incident neutron beam. Only reflection data were used, and data from detectors in line with the plane of the cell were discarded. Data were summed from several detectors corresponding to the scattering vector ( $Q$ ) range 2.0–2.3 Å<sup>-1</sup>. QENS measurements commenced 30 min after initial mixing, and the results were time-averaged over 33 min intervals. Data were collected continuously for up to 55 h. The incident neutron wavelength used was 4.8 Å. The energy resolution at the elastic line,  $\Delta E$ , is 0.146 meV.

### 2.3. Analyses and modeling of QENS data

The QENS spectra for the hydration reactions,  $S(Q, \omega)$ , was modeled in terms of four components, including Gaussian and Lorentzian peakshapes which have been demonstrated to describe the FCS QENS data for hydrating C<sub>3</sub>S [13,15,17,18,20–23]. These were as follows:

1. An elastic peak representing completely bound hydrogen was modeled using a resolution-limited Gaussian lineshape of width  $W_C$  and integrated area  $C$ .
2. The narrowest quasielastic-broadened component arising from pseudo-bound hydrogen was modeled using a Lorentzian lineshape of width  $W_P$  and integrated area  $P$ .
3. Two wider quasielastic-broadened components arising from hydrogen in the “free” water, modeled using Lorentzian lineshapes of widths  $W_{F_1}$  and  $W_{F_2}$ .

The peak analysis utility (PAN) within the data analysis and visualization environment (DAVE) [26] was used for the analyses of QENS data. The method is outlined in the Eq. (5). A  $\chi^2$  minimization process was used in this program.

$$S(Q, \omega) = \frac{C}{\sqrt{2\pi(W_C/2.354)^2}} e^{-\frac{1}{2}\left(\frac{x-x_0}{W_C/2.354}\right)^2} + \frac{W_P}{2\pi} \frac{P}{(x-x_0)^2 + (W_P/2)^2} + \frac{W_{F_1}}{2\pi} \frac{F_1}{(x-x_0)^2 + (W_{F_1}/2)^2} + \frac{W_{F_2}}{2\pi} \frac{F_2}{(x-x_0)^2 + (W_{F_2}/2)^2}, \quad (5)$$

where  $x$  is the energy transfer ( $\hbar\omega$ ) and  $x_0$  (which remained approximately 0) is the center for each peak. In all calculations,  $x_0$  was constrained to be the same for each component.  $W_{F_1}$  and  $W_{F_2}$  were determined from data for the first seven time-averaged slices (3.85 h), where all the water was assumed to be in the free-state, and the value was fixed

<sup>2</sup> Manufacturers are identified in order to provide complete identification of experimental conditions, and such identification is not intended as a recommendation by the University of Maryland, NIST, or Federal Highway Administration.

for subsequent fits. For this determination, an elastic line was included to account for the small contributions to the spectra from the unreacted tricalcium silicate grains, and the sample cell. In a similar manner,  $W_P$  was determined from the final seven time-averaged slices of reaction time, and the one Gaussian and three Lorentzian components were used in this determination.  $W_C$  was fixed to the instrument resolution. The average  $W_P$  determined from these last seven spectra was fixed for fits at previous reaction times. Thus, the five variables that were used in the fitting were  $x_0$ , and the four integrated areas  $C$ ,  $P$ ,  $F_1$  and  $F_2$ . Fig. 1 shows typical fitting of QENS data using DAVE.

The bound water index (BWI) is defined [15]

$$\text{BWI} = 1 - \text{FWI} = \frac{C + P}{C + P + F_1 + F_2}, \quad (6)$$

where FWI is the free water index. Using the BWI to observe the reaction, the nucleation and growth regime was modeled as a stretched exponential Eq. (7) [13]:

$$\text{BWI}(t) = \text{BWI}(i) + A[1 - \exp\{-[k(t - t_i)]^n\}], \quad (t_i \leq t \leq t_d). \quad (7)$$

In Eq. (7),  $\text{BWI}(t)$  is the BWI at time  $t$  and  $\text{BWI}(i)$  is the BWI at the nucleation and growth start time,  $t_i$ .  $k$  is the nucleation and growth reaction rate.  $A$  is the BWI after infinite time, and can be correlated with early strength [20,21]. The exponent  $n$  characterizes the dimensionality of product growth occurring in a three dimensional pore space. The value of  $n$  can be determined from QENS, although it is more precisely determined by calorimetry [27]. Thomas and Jennings [27] determined  $n$  for a range of monoclinic  $\text{C}_3\text{S}$  pastes prepared with  $\text{D}_2\text{O}$  and  $\text{H}_2\text{O}$  over 20–40 °C to vary only from 2.44 to 2.65. Although the differences between the  $n$  values for monoclinic and triclinic forms of  $\text{C}_3\text{S}$  have not been previously noted or commented upon, recent QENS and calorimetry studies have determined  $n$  for both these forms. Thomas and Jennings [27] determined monoclinic  $\text{C}_3\text{S}$  to be 2.65 at 30 °C. Fitz-

Gerald et al. [18] determined  $n$  to be 2.26 at 30 °C for triclinic  $\text{C}_3\text{S}$ , however, the form was not specified in this work, but later referred to as triclinic in work by co-researchers and others [17]. These studies [17,18,27] all use  $\text{C}_3\text{S}$  sourced from the same supplier as the current work and it is likely that the forms are the same as those used here. Hence, the literature values for triclinic and monoclinic  $\text{C}_3\text{S}$  forms suggest that the monoclinic has a greater dimensionality of growth than the triclinic form. In any case, the nucleation and growth model (7) is relatively insensitive to changes in  $n$  and modeling using  $n$  values of 2.27 and 2.65 for the triclinic sample made only a 0.8% alteration to  $A$  and 4% alteration to  $k$ . The errors reported are 2% in  $A$  and 4% in  $k$ . The errors propagated by changes in  $n$  for  $A$  and  $k$ , were hence found to be within the reported error for  $k$  and  $A$ . For these reasons,  $n$  was fixed to 2.65 in the modeling of both samples. The reaction rate,  $d(\text{BWI})/dt$ , peaks with a maximum approximately proportional to the product,  $\{nAk\}$ .

For a mono-dispersed population of  $\text{C}_3\text{S}$  particles with an initial un-reacted radius of  $R$ , a radius  $r$  after hydration time  $t$ , and a water to cement component mass ratio such that the free water is just consumed when the system is fully hydrated,  $\text{FWI}(t)$  is proportional to  $(r/R)^3$  [18]. Allen et al. [13] showed that during diffusion limited hydration (8):

$$[\text{FWI}(t)]^{1/3} = [\text{FWI}(t_d)]^{1/3} - (R^{-1})(2D)^{1/2}(t - t_d)^{1/2}. \quad (8)$$

In Eq. (8),  $D$  is an effective diffusion constant controlling water migration to the unhydrated  $\text{C}_3\text{S}$ , and has been linked to the permeability of the hydration layer.  $R^{-1}$  is the inverse radius of the hydrating particle.  $\text{FWI}(t_d)$  is the free water index predicted at the diffusion limited regime start time,  $t_d$ .

For polydispersed  $\text{C}_3\text{S}$ ,  $R$  must be averaged over the size distribution. Rewriting with BWI instead of FWI, Eq. (9) is produced [19]:

$$\text{BWI}(t) = \text{BWI}(i) + [1 - \{[1 - \text{BWI}(t_d)]^{1/3} - (R^{-1})(2D_i)^{1/2}(t - t_d)^{1/2}\}^3], \quad (t > t_d). \quad (9)$$

In Eq. (9),  $D_i$  is an amended effective diffusion coefficient taking into account the particle size distribution.  $R^{-1}$  is the mean inverse radius averaged over the unhydrated particle size distribution.  $\text{BWI}(t_d)$  is the bound water index predicted at the diffusion limited regime start time,  $t_d$ .

Eq. (9) was used to model the diffusion limited hydration just as Eq. (7) was used to model the nucleation and growth processes. The assumption that either nucleation and growth processes or diffusion limited processes were operative at any given hydration time was made.  $R^{-1}$  was determined from particle size distribution reports sent from CTL. Reports are based on an average of four particle size distribution measurements and the volume weighted average inverse radius was determined for each sample; this value was used in the modeling. For the mixtures, the  $R^{-1}$  corresponding to the dominant phase of the mixture was used.  $t_i$  was established from the QENS hydration

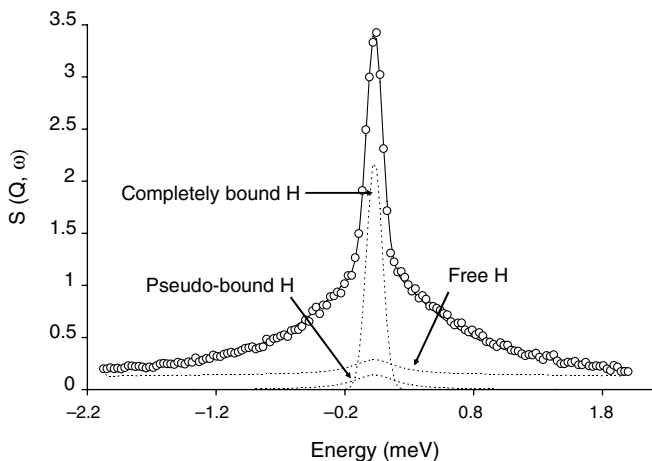


Fig. 1. Typical fitting of the QENS data at 5 h hydration time using DAVE, detailing the Gaussian and Lorentzian profiles as dotted lines. The overall fit through the data (○) is indicated by the solid line.

modeling and  $t_d$  was also established from these models from the narrow range that resulted in the smooth transition from nucleation and growth to diffusion limited kinetics. The parameters allowed to vary further in the model for the rest of the fitting were  $D_i$ ,  $A$ , and  $k$ .

#### 2.4. Particle size effects and differences in hydrating volume

The powder form of the different  $C_3S$  forms investigated here was obtained by processing larger chunks of the material. The different forms fracture and crush differently and obtaining identical particle size distributions for each form is impossible and was not attempted. The effects of particle size distributions on  $C_3S$  hydration over both nucleation and growth and diffusion limited hydration mechanics have been quantified using a single time-dependent model for QENS data over the full hydration time [13]. The effects of particle size distribution differences were initially interpreted in conjunction with this model, based on the particle size distribution affecting the volume of material available to the hydration, with respect to the amount of exposed surface for water to react. The model can be used to identify the effects on  $C_3S$  hydration caused by varying the initial particle size distribution of a given crystal form. Extension of this approach to extract differences among non-identical forms may not be appropriate, as there is evidence in the literature to suggest that the hydration mechanisms of these forms are significantly different. The hydration of monoclinic  $C_3S$  involves a more violent rupture of the C–S–H layer, described as the lifting and peeling of sheets [5], whereas triclinic C–S–H simply erupts as needle-like growths from the hydrating grain. These different mechanisms of hydration may result in different hydrating volumes, with the monoclinic form likely to have exposure of fresh  $C_3S$  surfaces during delamination processes. The observed delamination may arise due to the dislocations, strains, or distortions in the lattice of  $C_3S$  stabilized with a higher amount of Mg (monoclinic) previously observed to affect the nucleation and growth processes [7]. Other research [28] has determined that the rate limiting factors in  $C_3S$  hydration are independent of particle size distribution. The QENS and INS results here are interpreted with respect to the known effects of particle size and a consideration of the potential differences of hydration mechanisms of the two forms.

#### 2.5. Inelastic neutron scattering

The inelastic data were obtained using the NIST Center for Neutron Research Filter Analyzer Neutron Spectrometer (FANS) at BT-4 [29]. The sample was oriented, in reflection, at a  $45^\circ$  scattering angle. A Cu (220) monochromator was used, with pre and post collimation of  $60'$  and  $40'$ , respectively. Samples prepared identically to those of the QENS experiment were analyzed at  $30^\circ\text{C}$ . Hydration cells used were identical to those used for QENS experiments, and reflection geometry data only were used. Data

were collected over the energy range 25–55 meV. The reference spectra were measured for a known mass of pure  $\text{Ca}(\text{OH})_2$  powder placed in an identical experimental setup as the hydrating samples. The sample and reference spectra were obtained under nominally identical conditions to ensure precision in the  $\text{Ca}(\text{OH})_2$  absolute mass calibration. Measurement of the integrated intensity of the 41 meV peak enabled the absolute quantity of  $\text{Ca}(\text{OH})_2$  formed in the hydrated  $C_3S$  samples to be calculated. Background data consisting of an empty hydration cell were also collected.

#### 2.6. Analyses of inelastic neutron scattering data

The inelastic neutron scattering spectrum for each sample is representative of the density of states of the sample. DAVE [26] was used for the data reduction and analyses of the inelastic neutron scattering data. The spectrum for the  $\text{Ca}(\text{OH})_2$  standard was modeled using three Gaussian lineshapes, and a linear background, detailed in Fig. 2. The spectra for the hydrated  $C_3S$  forms were modeled using a single Gaussian lineshape due to the significantly lower counts resulting from the reduced  $\text{Ca}(\text{OH})_2$  amount in the sample relative to the standard.

### 3. Results and discussion

#### 3.1. XRF and particle size analyses

Mg and Al were found present in significant amounts in the monoclinic ( $M_3$ ) sample (Table 1).  $\text{Mg}^{2+}$  has been shown to substitute directly for  $\text{Ca}^{2+}$  in the  $C_3S$  lattice [30] and at concentrations above 1.35% Mg the monoclinic form can be stabilized at room temperature [5]. Below this amount, the  $T_1$  and  $T_2$  triclinic forms can be stabilized. The solubility limit of Mg in  $C_3S$  has been shown to be about 1.5 wt.% [2]. Al can be incorporated into  $C_3S$  to stabilize the  $T_1$  or  $T_2$  form up to 1 wt.% [4,31]. At amounts greater than 0.45 wt.% the  $T_2$  form is stabilized.  $\text{Al}^{3+}$  has been

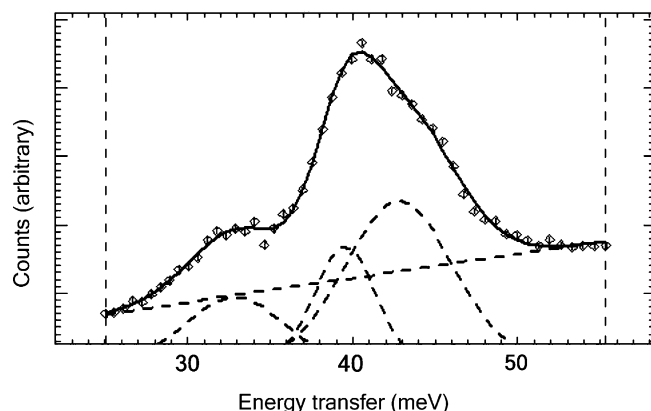


Fig. 2. Inelastic spectra for  $\text{Ca}(\text{OH})_2$  reference showing the three Gaussian and background components used in the fitting. The bold dotted lines represent the individual components, whilst the solid line represents the overall fit.

shown to substitute  $\text{Si}^{4+}$  in the structure [32]. The combination of  $\text{Al}^{3+}$  and  $\text{Mg}^{2+}$  influences the stabilization of the  $T_1$ ,  $T_2$ , and  $M_1$  forms through the mutual interactions of these ions [33]. The amount of one ion required for stabilization reduces with the increasing amount of the other ion and the addition of suitable atoms through this method enables the stabilization of higher monoclinic forms. The quantities of impurity ions present in the samples are therefore consistent with the stabilization of the  $T_1$  and  $M_3$  forms used in this study.

The monoclinic sample has a larger particle size diameter and lower specific surface area than the triclinic sample. The monoclinic had an average particle of  $34\text{ }\mu\text{m}$  and specific surface area of  $0.303\text{ m}^2\text{g}^{-1}$ , compared to the triclinic sample values of  $9.8\text{ }\mu\text{m}$  and  $0.533\text{ m}^2\text{g}^{-1}$ , respectively. The volume weighted average inverse radius was determined for each sample, and this value was used in the modeling. Particles smaller than  $1\text{ }\mu\text{m}$  were neglected for the  $\text{C}_3\text{S}$  samples, as the particle size results showed that less than 5.5% of the volume was present in particle sizes below this value. A summary of the particle size distribution for each form is shown in Table 2.

### 3.2. Interpretation of the QENS data

The following considerations of the initial particle size distribution were included in the interpretation of QENS data, taken from [13]. The length of the dormant or induction period ( $t_i$ ) and the kinetics of the nucleation and growth of the hydration product ( $k$ , and also determining  $t_d$ ) are independent of the particle size distribution. Initial particle size strongly affects the asymptotic limit of the amount of total hydrated product ( $A$ ), with finer particle sizes producing a larger value. The diffusion limited rate of hydration is known to be significantly determined by the initial particle size distribution, and increases with increasing particle size.

The BWI curves (Fig. 3) have several features of interest. In the case of the monoclinic sample, the broad tapering into the diffusion limited regime after the nucleation and growth regime is indicative of a broader initial particle size distribution [13], consistent with the particle size distribution report. In contrast, the triclinic sample exhibits an earlier transition between these two hydration mechanisms, also consistent with a narrower particle size distribution. This indicates that the monoclinic sample maintains its broader particle size into the diffusion limited hydration period and indicates that any delamination of the C–S–H does not completely destroy the hydrating  $\text{C}_3\text{S}$  particle. The parameters determined from the hydration models are shown in Table 3. The fits of the models to the data can be observed in Fig. 3.

The combination of kinetic parameters during the nucleation and growth regime is such that the increase of BWI with time is essentially linear up to the reaction peak [20–23]. This enables the slope,  $d(\text{BWI})/dt$ , to be approximated as a constant during this period. No significant difference

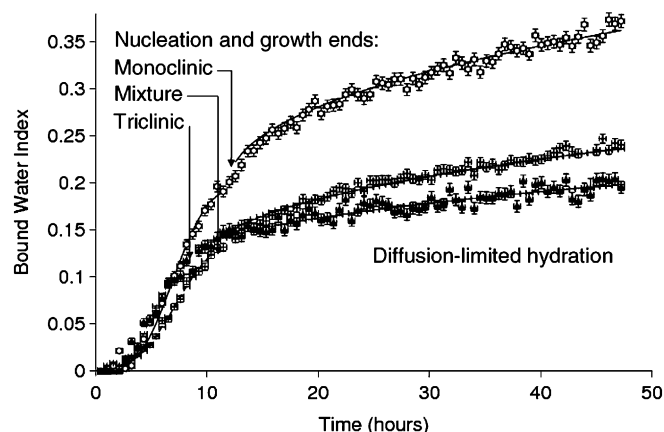


Fig. 3. Fits of hydration model to the BWI data for pastes of monoclinic (O, top), triclinic (▲, bottom), and a 1 to 1 monoclinic to triclinic mixture (+, center) of tricalcium silicate. Lines through the data represent the fit of the hydration models. Error bars represent absolute error.

between the rate of product formation for the triclinic and the monoclinic sample was noted (Table 3). This was not expected from the particle size distribution reports, where an increase in the  $d(\text{BWI})/dt$  of the larger surface area/smaller particle sized sample would be predicted by the associated increase in availability of  $\text{C}_3\text{S}$  to the water, if the intrinsic reactivities of the samples were the same. Considerations of the variations in hydrating volume for the two forms must be performed before a comparison of  $d(\text{BWI})/dt$  will give a reliable measure of relative reactivities with water. Any delamination of the C–S–H layer that formed in the case of the monoclinic sample would result in more  $\text{C}_3\text{S}$  for further nucleation and growth. This additional fuel may or may not offset the effects of the larger particle size. Hence,  $d(\text{BWI})/dt$  was not used as an indication for the reaction rate during the nucleation and growth as with previous studies [20–23].

While  $d(\text{BWI})/dt$  can be expected to suffer from the effects of  $\text{C}_3\text{S}$  availability to the hydration, the intrinsic reaction rate,  $k$ , is independent of these effects [13]. The values of  $k$  indicate that the monoclinic form is inherently less reactive, by about 33(4)%, than the triclinic form. This result is supported by the slightly longer induction period (23(8)% larger  $t_i$ ) observed for the monoclinic form. This result indicates that any mechanism of C–S–H rupture involving delamination of the C–S–H does not arise due to the increased reactivity of the monoclinic, compared to the triclinic, form. It is important to remember that the reaction rate,  $d(\text{BWI})/dt$ , peaks with a maximum approximately proportional to the product,  $\{nAk\}$ , and not simply  $k$  alone. As expected, the value for  $nAk$  was consistent with the trends for those reported in  $k$  (Table 3).

The monoclinic sample produced significantly more hydration product by the start of the diffusion limited hydration than the triclinic form, primarily as a result of an increase in the length of the nucleation and growth period, reflected in the increased value of  $t_d$  (Fig. 3). The model parameter  $A$  is determined from the nucleation

Table 3

Model parameters derived (except radius) for hydrated triclinic and monoclinic tricalcium silicate. Errors are in the last digit and represent one standard deviation

	$A$ (°)	$k$ (h <sup>-1</sup> )	$Akn$ (°h <sup>-1</sup> )	$d(BWI)/dt$ (°h <sup>-1</sup> )	$D_i$ (10 <sup>-15</sup> m <sup>2</sup> h <sup>-1</sup> )	$2D_i \times \langle R^{-1} \rangle^2$ (10 <sup>-5</sup> h <sup>-1</sup> )	$t_i$ (h)	$t_d$ (h)	Weighted average radius (×10 <sup>-6</sup> m)
Triclinic									
$n = 2.65$	0.104(2)	0.25(1)	0.073(3)	0.018(1)	0.28(3)	2.3(8)	1.3(1)	8.2(1)	4.9
$n = 2.27$	0.112(2)	0.24(1)	0.062(2)	0.018(1)	0.30(3)	2.5(8)	1.3(1)	8.2(1)	4.9
Monoclinic									
$n = 2.65$	0.193(5)	0.16(1)	0.082(3)	0.020(1)	19(2)	13(4)	1.6(1)	12.0(1)	17
Mixture									
$n = 2.65$	0.129(3)	0.14(1)	0.048(2)	0.016(1)	0.60(7)	5.0(2)	1.0(1)	11.0(1)	4.9
$n = 2.65$	0.129(3)	0.14(1)	0.048(2)	0.016(1)	7.0(8)	4.8(2)	1.0(1)	11.1(1)	17

<sup>a</sup> Units reflect those for BWI.

and growth model extrapolated to infinite time, although in reality the hydration mechanism becomes diffusion dominated after  $t_d$ . In a previous study of Mg-stabilized C<sub>3</sub>S [2], the amount of reacted C<sub>3</sub>S during hydration was decreased by the addition of MgO during manufacture of the C<sub>3</sub>S (pure C<sub>3</sub>S, 0.5 wt.% and 1.0 wt.% MgO) until a level above which stabilization of the monoclinic form was possible (2.0 wt.% MgO), where a sharp increase in the amount of reacted C<sub>3</sub>S was observed. Another study of Ti-stabilized C<sub>3</sub>S showed that the monoclinic form (4% TiO<sub>2</sub>) exhibited a higher percentage of hydration, in terms of the percentage of C<sub>3</sub>S reacted, when compared to pure C<sub>3</sub>S or triclinic forms stabilized with smaller amounts of Ti [1]. This study therefore corroborates the literature results and indicates that the percentage of hydration may be linked to the crystal form.

The monoclinic sample has a larger effective diffusion coefficient,  $D_i$ , which has been shown to increase with increasing particle size [13]. This previous study determined that for C<sub>3</sub>S, a difference of average particle size such as in this study would be expected to give a difference of  $3 \times 10^{-15}$  m<sup>2</sup> h<sup>-1</sup>, however, a difference of  $18.7 \times 10^{-15}$  exists, indicating a  $D_i$  value approximately ten times larger than what would be expected if only that particle size difference was the cause. The effective diffusion limited reaction constant, found by the calculation  $2D_i \times \langle R^{-1} \rangle^2$ , has been shown to have a different variation with particle size than for  $D_i$ . Fine particles were found to enhance the diffusion limited rate constant due to the geometric effect of decreased distance over which water must migrate to reach the unhydrated particles [13]. At 30 °C, the effect of a reduction in particle size results in a slight increase in this value. The significant increase in the effective diffusion limited rate constant here demonstrates the alteration to C–S–H morphology.  $D_i$  has been linked to the permeability of the C–S–H layer, which is affected by the layer's structure and morphology. The increase in  $D_i$  and the effective diffusion limited rate constant for the monoclinic form are consistent with an increase in permeability of the C–S–H layer of the monoclinic, relative to the triclinic, form. In these C<sub>3</sub>S samples, such differences may arise from the rate of dissolution, presumably of calcium and a small number

of magnesium ions, diffusing from the dissolving grain, leaving grain surfaces with varying degrees of silicate rich surface layers. This may account for the alteration to the morphology resulting in increased permeability of the C–S–H layer produced by the monoclinic form. Earlier research has also noted that the type of product that forms varies when different stabilizing ions are used in C<sub>3</sub>S samples [7]. An increase in the permeability of the hydration layer of the monoclinic form is attributed here as the likely cause for the increase in the length of the nucleation and growth regime as a result of a slower change to diffusion limited mechanics.

### 3.3. Interpretation of the hydrated polymorphic mixture

The shape of the BWI curve for the mixture illustrates a broad transition from nucleation and growth into the diffusion limited regime, indicative of the broad particle distribution of the mixture (Fig. 3).

As expected, the values of  $t_d$ ,  $D_i$ , the effective diffusion limited rate constant, and  $A$  for the mixture lies midway between the values for the individual forms.

Curiously,  $t_i$  and  $k$  for the mixture were lower than for either individual form. This suggests that there is an interaction that affects the hydration rate during the nucleation and growth regime, an effect that is not as simple as a linear combination of the C<sub>3</sub>S forms. Possible mechanisms for this result include a variation in the morphologies of the products formed by the two crystal forms and a variation in the solution chemistry arising from dissimilar dissolution rates of the two forms.

### 3.4. Inelastic neutron scattering quantification of Ca(OH)<sub>2</sub>

Inelastic neutron scattering data was averaged for each hydrating C<sub>3</sub>S form during the hydration period of 22–24 h. From the QENS BWI curves, this corresponded to the diffusion limited hydration regime, where the Ca(OH)<sub>2</sub> amount would not be expected to vary rapidly. Fig. 4 shows the inelastic neutron scattering spectra for the monoclinic (top of Fig. 4) and triclinic (bottom of Fig. 4) forms. Differences in the sample and reference spectra are thought to

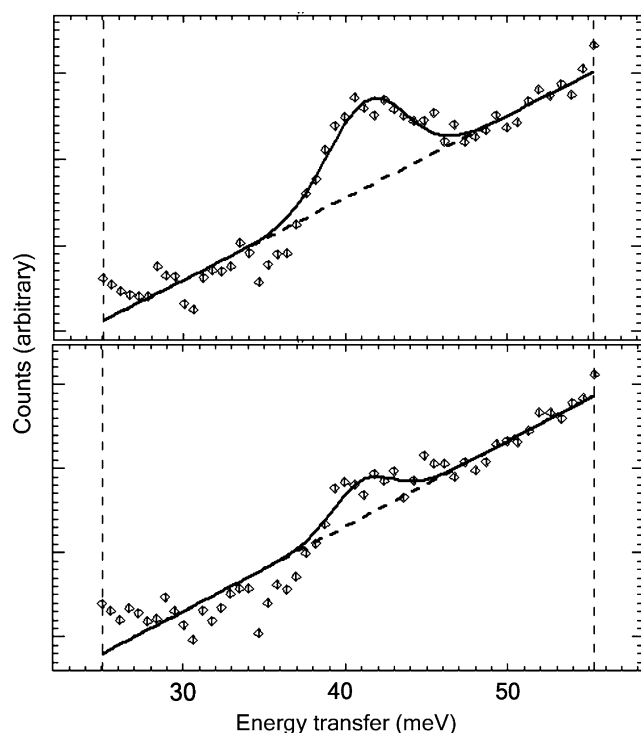


Fig. 4. Inelastic spectra for hydrating monoclinic (top) and triclinic (bottom) tricalcium silicate at 23 h. The solid line represents the overall fit.

arise from contributions from the C–S–H, and the significantly reduced  $\text{Ca(OH)}_2$  quantity of the sample spectra relative to the reference. Comparison of the  $\text{Ca(OH)}_2$  standard with the monoclinic and triclinic  $\text{C}_3\text{S}$  samples revealed significant differences in the quantity of  $\text{Ca(OH)}_2$  produced. The monoclinic sample made approximately  $2.0(2) \times 10^{-3}$  mol  $\text{Ca(OH)}_2$  from  $1.2451(2) \times 10^{-2}$  mol  $\text{Ca}_3\text{SiO}_5$ , and the triclinic sample  $6.9(7) \times 10^{-4}$  mol  $\text{Ca(OH)}_2$  from  $1.2485(2) \times 10^{-2}$  mol  $\text{Ca}_3\text{SiO}_5$ , at the same water to cement component ratios. Despite having almost half the initial surface area of the triclinic sample, the monoclinic sample produced almost three times the amount of  $\text{Ca(OH)}_2$ . Hence, these results agree with the QENS results, which ultimately predicted that more products would be made by the monoclinic sample, primarily through the delayed onset of diffusion limited hydration in the monoclinic case.

A study on Mg-stabilized  $\text{C}_3\text{S}$  indicated that the  $\text{Ca(OH)}_2$  produced by hydrating triclinic  $\text{C}_3\text{S}$  samples increased with increasing MgO amounts [2]. Unfortunately, only one sample with a higher amount of Mg was tested in this study, and this sample exceeded the solubility limit of Mg in  $\text{C}_3\text{S}$ . Another study investigated Ti-stabilized  $\text{C}_3\text{S}$ , and found that monoclinic samples produced a larger amount of  $\text{Ca(OH)}_2$  at any time [1]. The results of this INS study are therefore in agreement with the literature studies.

#### 4. Conclusions

The differences in hydration mechanics between a triclinic and monoclinic tricalcium silicate form stabilized

with Mg were characterized. The key findings were that the monoclinic form was less reactive than the triclinic form, although it was found to produce more product after 50 h. This process was found to occur primarily though longer, and not earlier, nucleation and growth regime. The increased nucleation and growth length was attributed to an increase in the permeability of the monoclinic product relative to that produced by the triclinic form resulting in a slower change to diffusion limited hydration mechanics.

#### Acknowledgments

Thanks to Dr. Dan A. Neumann and Juscelino Leão from the National Institute of Standards and Technology (NIST) Center for Neutron Research. We are grateful to Dr. Andrew J. Allen from the Materials Science and Engineering Laboratories at NIST for previous work and discussions on particle size effects. We acknowledge the support of the National Institute of Standards and Technology, US Department of Commerce, in providing the neutron research facilities used in this work.

#### References

- [1] N.K. Katyal, S.C. Ahluwalia, R. Parkash, *Cement Concrete Res.* 29 (1999) 1851.
- [2] N.K. Katyal, S.C. Ahluwalia, R. Parkash, *Cement Concrete Res.* 28 (1998) 867.
- [3] V.S. Ramachandran, J.J. Beaudoin, S.L. Sarkar, X. Aimin, *Cemento* 90 (1993) 73.
- [4] W. Nocuń-Wcelik, B. Trybalska, *J. Thermal Anal.* 32 (1987) 1719.
- [5] H.R. Stewart, J.E. Bailey, *J. Mater. Sci.* 18 (1983) 3686.
- [6] G.L. Valentini, V. Sabatelli, B. Marchese, *Cement Concrete Res.* 8 (1978) 61.
- [7] G. Mascolo, V.S. Ramachandran, *Mater. Constr.* 8 (1975) 373.
- [8] R.A. Thompson, D.C. Killoh, J.A. Forrester, *J. Am. Ceram. Soc.* 58 (1975) 54.
- [9] T. Harada, A. Ohta, S. Takagi, *Rev. Gen. Meet., Tech. SE SS – Cement Assoc. Jpn.* 31 (1977) 31.
- [10] T. Staněk, P. Sulovský, *Cement Concrete Res.* 32 (2002) 1169.
- [11] H.F.W. Taylor, *Cement Chemistry*, Thomas Telford, London, 1997.
- [12] P. Barret, D. Bertrandie, *J. Chim. Phys.* 83 (1986) 765.
- [13] A.J. Allen, J.C. McLaughlin, D.A. Neumann, R.A. Livingston, *J. Mater. Res.* 19 (2004) 3242.
- [14] D.P. Bentz, E.J. Garboczi, C.J. Haecker, O.M. Jensen, *Cement Concrete Res.* 29 (1999) 1663.
- [15] S.A. FitzGerald, J.J. Thomas, D.A. Neumann, R.A. Livingston, *Cement Concrete Res.* 32 (2002) 409.
- [16] E. Fratini, S.-H. Chen, P. Baglioni, M. Bellissent-Funel, *Phys. Rev. E* 64 (2001). Art. No. 020201.
- [17] J.J. Thomas, S.A. FitzGerald, D.A. Neumann, R.A. Livingston, *J. Am. Ceram. Soc.* 84 (2001) 1811.
- [18] S.A. FitzGerald, D.A. Neumann, J.J. Rush, D.P. Bentz, R.A. Livingston, *Chem. Mater.* 10 (1998) 397.
- [19] S.A. FitzGerald, D.A. Neumann, J.J. Rush, R.J. Kirkpatrick, X. Cong, R.A. Livingston, *J. Mater. Res.* 14 (1999) 1160.
- [20] V.K. Peterson, D.A. Neumann, R.A. Livingston, *J. Phys. Chem. B* 109 (2005) 14449.
- [21] V.K. Peterson, D.A. Neumann, R.A. Livingston, *Mater. Res. Soc. Symp. Proc.* 840 (2004) Q2.2.
- [22] V.K. Peterson, D.A. Neumann, R.A. Livingston, *Chem. Phys. Lett.* 419 (2005) 16.

- [23] V.K. Peterson, D.A. Neumann, R.A. Livingston, *Physica B* (in press).
- [24] J.J. Thomas, J.J. Chen, H.M. Jennings, *Chem. Mater.* 15 (2003) 3813.
- [25] J.R. Copley, T.J. Udovic, *J. Res. Natl. Inst. Stand. Technol.* 98 (1993) 71.
- [26] DAVE, National Institute of Standards and Technology Center for Neutron Research.
- [27] J.J. Thomas, H.M. Jennings, *Chem. Mater.* 11 (1999) 1907.
- [28] P.W. Brown, *J. Am. Ceram. Soc.* 72 (1989) 1829.
- [29] T.J. Udovic, D.A. Neumann, J. Leão, C.M. Brown, *Nucl. Instr. Meth. A.* 517 (2004) 189.
- [30] E. Woermann, W. Eysel, T. Hahn, *Zem-Kalk-Gips* 21 (1968) 241.
- [31] M. Bigaré, A. Guinier, C. Mazières, M. Regourd, N. Yannakis, W. Eysel, T. Hahn, E. Woermann, *J. Am. Ceram. Soc.* 51 (1967) 609.
- [32] J. Skibsted, H.J. Jakobsen, C.J. Hall, *Chem. Soc. Faraday Trans.* 90 (1994) 2095.
- [33] T. Hahn, W. Eysel, E. Woermann, in: *Proceedings of the 5th International Symposium on the Chemistry of Cement*, vol. 1, 1969, p. 61.